IOP Publishing Physics in Medicine and Biology

Phys. Med. Biol. **52** (2007) 5831–5854 doi:10.1088/0031-9155/52/19/007

Inferential modeling and predictive feedback control in real-time motion compensation using the treatment couch during radiotherapy

Peng Qiu[1], **Warren D D'Souza**[2], **Thomas J McAvoy**[3] **and K J Ray Liu**[1]

[1] Department of Electrical and Computer Engineering, University of Maryland, College Park, MD 20742, USA
[2] Department of Radiation Oncology, University of Maryland School of Medicine, Baltimore, MD 21201, USA
[3] Department of Chemical Engineering, University of Maryland, College Park, MD 20742, USA

E-mail: wdsou001@umaryland.edu

Received 8 December 2006, in final form 12 August 2007
Published 14 September 2007
Online at stacks.iop.org/PMB/52/5831

Abstract

Tumor motion induced by respiration presents a challenge to the reliable delivery of conformal radiation treatments. Real-time motion compensation represents the technologically most challenging clinical solution but has the potential to overcome the limitations of existing methods. The performance of a real-time couch-based motion compensation system is mainly dependent on two aspects: the ability to infer the internal anatomical position and the performance of the feedback control system. In this paper, we propose two novel methods for the two aspects respectively, and then combine the proposed methods into one system. To accurately estimate the internal tumor position, we present partial-least squares (PLS) regression to predict the position of the diaphragm using skin-based motion surrogates. Four radio-opaque markers were placed on the abdomen of patients who underwent fluoroscopic imaging of the diaphragm. The coordinates of the markers served as input variables and the position of the diaphragm served as the output variable. PLS resulted in lower prediction errors compared with standard multiple linear regression (MLR). The performance of the feedback control system depends on the system dynamics and dead time (delay between the initiation and execution of the control action). While the dynamics of the system can be inverted in a feedback control system, the dead time cannot be inverted. To overcome the dead time of the system, we propose a predictive feedback control system by incorporating forward prediction using least-mean-square (LMS) and recursive least square (RLS) filtering into the couch-based control system. Motion data were obtained using a skin-based marker. The proposed predictive feedback control system was benchmarked against pure feedback control (no forward prediction) and resulted in a significant performance gain. Finally, we combined the PLS inference model and the predictive feedback control to evaluate the overall

performance of the feedback control system. Our results show that, with the tumor motion unknown but inferred by skin-based markers through the PLS model, the predictive feedback control system was able to effectively compensate intra-fraction motion.

1. Introduction

Sophisticated respiration-induced tumor motion correction strategies that do not result in an increase in treatment time (or reduction in duty cycle) involve real-time motion compensation. The Cyberknife system (Accuray Inc., Sunnyvale, CA) (Schweikard *et al* 2000, 2004, Chang and Adler 2001, Ozhasoglu and Murphy 2002, Murphy 2004) is currently the only clinically implemented real-time system. However, there are two additional proposed systems using the multileaf collimator (MLC) (Keall *et al* 2001, 2006, Papiez 2004, Papiez and Rangaraj 2005, Webb 2005, Papiez *et al* 2005) and the treatment couch (D'Souza *et al* 2005, D'Souza and McAvoy 2006), respectively, that have the potential to perform real-time motion compensation. The latter two systems have the advantage of being integrated with a conventional linear accelerator and the potential for overcoming some of the limitations of other clinically implemented motion correction methods. In this work, we focus on a motion compensation system based on the treatment couch. The performance of the real-time motion compensation control system depends on (1) the reliable estimation of internal tumor position and (2) the ability to overcome system dead time (latency) within the feedback control system.

Tumor position can be determined directly by (1) tracking the position of the fiducials implanted in or near the tumor, or by (2) tracking the positions of tumor surrogates and inferring the position of the tumor. In the first approach, a 2 mm gold fiducial marker is placed in or near the tumor and tracked using a set of four stereoscopic x-ray imagers (Imura *et al* 2005, Onimaru *et al* 2005, Seppenwoolde *et al* 2002, Shimizu *et al* 2002, Shirato *et al* 2000a, 2000b). A newer electromagnetic technology that consists of implanted beacon transponders has recently emerged (Calypso Medical Technologies, Seattle, WA). Implanting fiducials though, may find limited application in patients particularly those with compromised pulmonary capabilities due to the inherent risk for pneumothorax, bleeding and infection (Naruke and Koketsu 1981, Covey *et al* 2004, Kinoshita *et al* 2006).

In the second approach external surrogates are used to infer the position of the tumor in real-time. This approach has been adopted by the Cyberknife system in which a set of three light-emitting diodes is visualized by a camera system and tracked continuously. A linear correlation model is established between these LEDs and implanted fiducials based on periodically acquired x-ray images. Vedam *et al* (2000, 2001) have described a linear relationship between the diaphragm position and an optical reflector block (RPM system, Varian Medical Systems, Palo Alto, CA) placed on the abdomen of the patient based on retrospective evaluation. Isaksson *et al* (2005) have demonstrated a similar relationship between the positions of chest markers with the positions of fiducials implanted in the tumor. In a recent study, Yan *et al* (2006) investigated a multiple linear regression model to generate a composite signal from multiple external markers in order to predict the internal target motion. It was found that the mean correlation between the composite and internal signals was improved when more external signals were considered. This suggests that (1) there is a correlation between internal anatomical and external marker displacements and (2) multiple external signals might be an improved way to predict internal target motion compared with a single external signal.

Another problem to contend with in a feedback control system is the system dynamics and dead time (the time it takes for the couch system to begin to respond to a change in the input). While the dynamics of a couch system can be improved with faster actuators, the system dead time (latency) will inevitably cause a delay between the position of the tumor and the corrective position of the couch. In order to synchronize the position of the tumor and the corrective position of the couch, it is necessary to predict respiration-induced tumor displacement in advance. Further compounding the problem is the variation in respiration signals from one cycle to another (Seppenwoolde *et al* 2002). As described by Murphy (2004), there are two broad methods to predict the respiration: (1) a mathematical model that represents the respiration signal as a parameterized periodic function and (2) adaptive filtering which attempts to predict the future based on past history.

Autoregressive (AR) modeling is a powerful tool to model asymptotic stationary stochastic processes (Haykin 1996). Linear prediction has been previously used in speech signal processing (Deller *et al* 2000). Previous reports have determined the feasibility of forward-predicting the respiration signal and are briefly summarized here. Vedam *et al* (2004) performed a comparative analysis on prediction errors using a sinusoidal model and a least-mean-square (LMS) filter and found that the LMS filter outperformed the sinusoidal model for response times of less than 0.4 s. Isaksson *et al* (2005) investigated the use of neural networks in predicting the actual motion of the tumor using fluoroscopy images and benchmarked it against a linear filter. They found that by dynamically adjusting the parameters of the neural network, one could achieve better tumor tracking accuracy than linear filters. Sharp *et al* (2004) used several empirical models to predict respiratory motion including linear filters, neural networks and Kalman filtering. Murphy and Dieterich (2006) have compared the performance of linear and nonlinear adaptive neural networks for predicting irregular respiration signals.

Prediction of the respiration signal itself (as in most previous studies) is only useful for open-loop strategies such as gating. In real-time motion compensation systems (which are feedback systems), closed-loop and not open-loop respiration signal prediction needs to be studied within the context of the overall system performance. The incorporation of the prediction of the respiration signal into a real-time feedback control system and the resulting control system performance have not been investigated. D'Souza and McAvoy (2006) have previously performed an analysis of the treatment couch and control system dynamics for a real-time motion compensation couch using patient-derived respiration signals. Some of the previously published reports (though not all) have considered dead time in their discussions (but not explicitly in their simulations), though not the dynamics of the couch, MLC or robot-controlled linac. The question that remains to be answered is whether forward prediction methods can improve the performance of a feedback control system by overcoming the system dead time.

In this paper, we perform three tasks. (1) We describe a method to correlate in real time the positions of skin markers with the diaphragm position using partial-least-squares (PLS) regression using a limited 'training' data set. The method is evaluated by determining the error in inferring the real-time diaphragm position using external surrogates. (2) We determine the ability to predict the respiration signal using adaptive filtering methods: least-mean-square (LMS) filtering and recursive-least-square (RLS) filtering. Furthermore, we propose a predictive feedback control system that incorporates these adaptive filtering techniques into a previously described feedback control system for a real-time motion compensation couch system. The results from the predictive feedback control system are benchmarked against a pure feedback control system (with no forward prediction). (3) We then integrate both the PLS inference model and the predictive feedback control system. Based on the positions of the external skin markers, the position of the internal anatomy is inferred. With the estimated

internal tumor position, the predictive feedback control system is applied to overcome the dead time by predicting future anatomical motion, and the overall performance of the control system is evaluated.

2. Methods and materials

This section is organized as follows. We first propose the use of PLS regression to infer the diaphragm position based on the multiple external skin marker positions. Next, we describe forward prediction using the LMS and RLS filters, and their incorporation into a feedback control system using the treatment couch to overcome the system dead time. Finally, we combine the PLS inferential model and the forward prediction into an inferential predictive feedback control system.

2.1. Inferential modeling of the diaphragm using external surrogates

PLS is an ideal tool for applications in which there are many variables that can be used to predict one or more responses, i.e., there are multiple measured variables ('inputs') that can be used to predict the responses of other variables ('responses') (Lorber *et al* 1987, Wold *et al* 1994). PLS has found successful application in economics, chemometrics and medical imaging. While MLR can be used for similar applications, it can break down when the number of variables is large, and the variables are redundant, i.e., collinear. While MLR may fit the sampled data well, it can fail to predict any new data well due to 'over-fitting'. In such cases, even though the number of input variables is large there are probably only a few 'latent variables' (LVs) that account for most of the variation in the response(s). Methods like PLS are able to overcome this problem by performing the regression on a small number of orthogonal LVs, which are linear combinations of the original variables. The underlying idea of PLS is to extract these 'latent factors' that account for much of the variation in the inputs and responses while predicting the responses well.

2.1.1. Partial-least-squares (PLS) regression. The PLS algorithm may be described as follows (de Jong 1993). Consider a matrix $\boldsymbol{X}$ (predictor matrix) that contains m observations and n variables, and a matrix $\boldsymbol{Y}$ (response matrix) that contains m responses and r variables. At each stage, PLS calculates two latent variables: $\boldsymbol{t}_j$, a linear combination of the original $\boldsymbol{X}$ matrix variables and $\boldsymbol{u}_j$ a linear combination of the $\boldsymbol{Y}$ variables. These variables are chosen such that the covariance between $\boldsymbol{t}_j$ and $\boldsymbol{u}_j$ is maximized. $\boldsymbol{u}$ is set equal to a column of $\boldsymbol{Y}$. A weight matrix, $\boldsymbol{w}$, is then calculated by regressing the columns of $\boldsymbol{X}$ on $\boldsymbol{u}$. $\boldsymbol{w}$ is then normalized to the unit length. The score matrix $\boldsymbol{t}$ is calculated as $\boldsymbol{t} = \boldsymbol{X}\boldsymbol{w}/\boldsymbol{w}^T\boldsymbol{w}$. A loading matrix $\boldsymbol{q}$ is then calculated as $\boldsymbol{q}^T = \boldsymbol{t}^T\boldsymbol{Y}/\boldsymbol{t}^T\boldsymbol{t}$ by regressing the columns of $\boldsymbol{Y}$ on $\boldsymbol{t}$. A new $\boldsymbol{u}$ vector is then calculated as $\boldsymbol{u} = \boldsymbol{Y}\boldsymbol{q}/\boldsymbol{q}^T\boldsymbol{q}$. The convergence is then checked for $\boldsymbol{u}$. If convergence is determined then the loading matrix, $\boldsymbol{p}$, can be calculated as $\boldsymbol{p} = \boldsymbol{X}^T\boldsymbol{t}/\boldsymbol{t}^T\boldsymbol{t}$. If convergence is not determined, then the process is repeated starting with the calculation of the weight matrix $\boldsymbol{w}$. If convergence is determined, then residual matrices are calculated as $\boldsymbol{E} = \boldsymbol{X} - \boldsymbol{t}\boldsymbol{p}^T$ and $\boldsymbol{F} = \boldsymbol{Y} - \boldsymbol{t}\boldsymbol{q}^T$. If additional PLS dimensions (or LVs) are necessary, then the $\boldsymbol{X}$ and $\boldsymbol{Y}$ matrices are replaced by $\boldsymbol{E}$ and $\boldsymbol{F}$ and the calculation is repeated.

2.1.2. Data acquisition. Five patients underwent a fluoroscopy session to assess the extent of the diaphragm motion. Skin markers in the form of radio-opaque markers were placed at four locations on the patient's skin. The locations of the skin markers were as follows: xyphoid

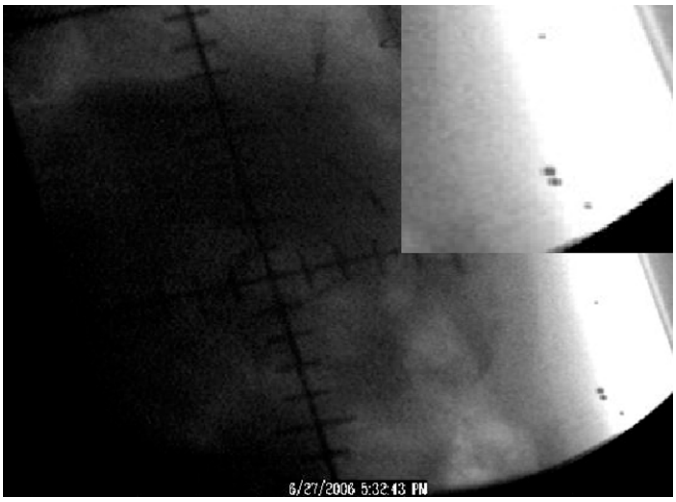

Figure 1. Fluorosocopy image of the diaphragm with skin markers placed on the abdomen of the patient from the lateral direction. The insert in the top right corner shows a magnified view of the four radio-opaque markers.

process (M1), approximately half-way between the xyphoid process and the umbilicus (M2), approximately 5–7 cm lateral to the M2 (M3 and M4). Fluoroscopy images were recorded at a frame rate of 3 frames s^{-1} from the lateral direction using a SL simulator (Elekta Oncology Systems, Norcross, GA) for a duration of 40–60 s using a frame grabber (ImperX Video Capture Essentials, Boca Raton, FL). Figure 1 shows a lateral view of the diaphragm and radio-opaque markers placed on the patient's abdomen. The number of marker coordinate and diaphragm position observations (i.e., m) per patient ranged from 130 to 160. Since we considered the 2D coordinates of four markers in this study, n was 8. We assessed a single output response, i.e., the superior–inferior (S–I) position of the diaphragm and therefore r was 1.

Distortion in the fluoroscopic images was corrected by implementing a second-order 2D polynomial similar to the distortion correction published by Gronenschild (1999) to correct for global spatial distortion. If uncorrected, distortion can lead to errors in the identification of the coordinates of the markers and diaphragm. Edge detection was used to aid in the identification of the diaphragm location. The coordinate of the diaphragm in the S–I direction (at the same anterior–posterior coordinate) and the coordinates of the markers were determined manually. The uncertainty of the measurement was estimated to be 0.5 mm based on repeated measurements of the diaphragm and marker coordinates by the same observer.

2.1.3. Cross-validation. The number of PLS LVs required to predict the responses well and not overfit the data is determined by cross-validation. In this process, the data set is divided into subsets and a new PLS model is generated using all but one of the subsets. The model is then used to predict $\boldsymbol{Y}$ and the prediction error sum of squares (PRESS) for the excluded subset is calculated as a function of the number of LVs. This procedure is repeated until all of the subsets have been deleted once. The PRESS values for each subset are summed to obtain a cumulative PRESS. This process is repeated with a different number of LVs. When the number of LVs equals the number of input variables, PLS regression is equivalent to MLR.

The duration over which imaging data are acquired typically comprises a fraction of the total treatment time. It is advantageous to decrease the temporal length of the training data session in order not to increase the overall treatment time. Therefore, any inferential method must be capable of building a robust model based on a small training data set and predict the internal anatomical position during the course of the treatment fraction. However, here we consider a very limited data set (approximately 10% of the total information) upon which to build a PLS model and then use the model to predict future diaphragm displacements.

The data were first divided into 10 contiguous blocks. The data were pre-processed by mean-centering only and by mean-centering and scaling to unit variance the coordinates of the skin markers and diaphragm. The purpose of scaling to unit variance is to 'equalize' the effects of all input variables in the $\boldsymbol{X}$ block. For example, consider two input variables with one marker displaying vastly greater displacement than the other. Without scaling to the unit variance the marker with a greater displacement might influence the diaphragm position to a greater extent than the marker with a smaller displacement.

Since respiration patterns vary during the course of a treatment fraction, we treated each of the contiguous blocks as a 'training' data set in our simulation (one at a time). Cross-validation was then performed on each 'training' data set. The 'training' data set corresponded to the observations used to build the model that can be used to predict future observations. The ensuing PLS model using the number of LVs from the cross-validation process was then used to predict the diaphragm position corresponding to the remainder of the fluoroscopic session (this included all observations other than those in the 'training' data set). To perform cross-validation, we divided each 'training' data set (consisting of 13–16 observations) into five contiguous blocks and the cumulative PRESS was determined as a function of the number of latent variables. The cross-validation process was repeated by dividing each 'training' data set into five random blocks. Since there were 13–16 data points in each training set and the data were split into five blocks, the PLS regression model was built by dropping two–three points (contiguous or random) and then evaluated for these dropped points. The number of LVs corresponding to the minimum cumulative PRESS was generally considered the optimal number of latent variables for the PLS model. In each case, the eight independent variables (2D coordinates corresponding to the four radio-opaque markers) comprised the columns of the X matrix (the number of rows corresponded to the number of observations). The Y matrix consisted of the S–I position of the diaphragm.

2.1.4. Diaphragm position prediction. Using the number of latent variables determined from the cross-validation process, the PLS regression model built with each training data set was then used to predict the S–I diaphragm position corresponding to the observations in the remaining data set. As a consequence, we used 13–16 data points and the number of LVs determined from the cross-validation process to predict the location of the remaining 117–144 diaphragm locations in each simulation. We benchmarked the performance of the PLS regression with standard multiple linear regression (MLR) (Yan *et al* 2006) for each of the 'training' data sets and patient cases. The MLR equation takes the form:

$$y_i = b_1 x_{1i} + b_2 x_{2i} + \cdots + b_n x_{ni} \tag{1}$$

where y_i is the diaphragm position of the ith observation, and $x_{1i}, x_{2i}, \ldots, x_{ni}$ are the coordinates of the sensors, and $b_1, b_2, \ldots, b_n$ are the regression coefficients (note that when the data are mean-centered the intercept is 0 and therefore is not included above). The solution of the above equation using least-squares fitting yields a set of regression coefficients. The error between the measured and predicted diaphragm positions was quantified using the mean of the absolute error and the standard deviation of the error for both the PLS and MLR models.

To test the robustness of PLS, we evaluated the prediction errors by considering different subsets of the entire data set as the 'training' data set since in a clinical environment any one of those data sets can correspond to data from which a robust skin marker-internal anatomy model must be built.

2.2. Predictive feedback control

To overcome system dead time in a feedback control system, it is desirable to be able to predict the respiration signal in advance and therefore, we propose a predictive feedback control system for real-time tumor motion compensation. The predictive feedback control system is simulated by incorporating forward prediction into a feedback control system using the treatment couch. In this section, we assume that the external skin surrogate is an exact surrogate for tumor motion. Furthermore, only 1D motion is considered but the methods described here can be extended to three dimensions.

2.2.1. Motion data. Tumor surrogate motion data were obtained using the Varian RPM system (Varian Medical Systems, Palo Alto, CA) in which the marker was placed on the patient's abdomen between the xyphoid process and the umbilicus. The marker displacement was recorded at a sampling period of 33.37 ms for 300 s using an infrared camera. Data obtained from 12 patients were used in this work. The mean displacement of the reflector was subtracted from the instantaneous displacement of the reflectors and analysis was performed on the resulting displacement trajectory.

2.2.2. Forward prediction of the respiration signal. Autoregressive (AR) modeling is a powerful tool to model asymptotic stationary stochastic processes, and to perform forward prediction. In this work, we apply it to model the respiration disturbance signals. We model the respiration signal as a discrete time random process $d(i)$, where i is the index of the sampling time point. Because of the correlations between different time points in the respiration signal, the current and past time points contain a certain amount of information about the future time points. An AR model utilizes the correlation and predicts the value of the future time point using a linear combination of the values of the current and past time points. We can predict the lth future point of the respiration signal as follows:

$$\hat{d}(i+l) = \sum_{j=0}^{K-1} \omega_j d(i-j), \tag{2}$$

where, ω_j's are the model coefficients, and K is the order of the AR model.

To achieve the forward prediction, we need to find a set of coefficients ω_j that minimize the prediction error, the difference between the true respiration signal $d(i+l)$ and the predicted signal $\hat{d}(i+l)$. In practice, since the subject's respiration pattern may change during the treatment, the optimal values of coefficients ω_j may change over time. Therefore, in order to estimate the time-varying coefficients ω_j, adaptive schemes have to be employed. In adaptive filtering schemes, in order to dynamically track the time-varying system, the model coefficients ω_j are updated at each time point, based on the newly observed respiration signal. In this study, we examine two adaptive filtering schemes: (1) LMS and (2) RLS.

The LMS algorithm estimates the model coefficients ω_j based on a gradient search. The summary of the LMS algorithm is as follows. Let $\mathbf{d}(i) = [d(i), d(i-1), \ldots, d(i-K+1)]^T$ and let $\hat{\mathbf{w}}_l(i) = [\hat{\omega}_0(i), \hat{\omega}_1(i), \ldots, \hat{\omega}_{K-1}(i)]^T$ be the estimated AR coefficients at time point i. For every iteration, when a new time point is observed,

- given the value of the coefficients $\hat{\mathbf{w}}_l(i)$ (either from initialization or the previous iteration), the predicted respiration signal is $\hat{d}(i+l) = \hat{\mathbf{w}}_l^H(i)\,\mathbf{d}(i)$;
- the prediction error is $e(i) = d(i+l) - \hat{d}(i+l)$;
- the model coefficient is updated $\hat{\mathbf{w}}_l(i+1) = \hat{\mathbf{w}}_l(i) + \mu\,\mathbf{d}(i)e^*(i)$;

where μ is a constant, the learning rate of the LMS algorithm. If the value of μ is small, the convergence rate of the LMS algorithm is slow. On the other hand, if the value of μ is too large, the LMS algorithm diverges. In our study, respiration signals from 12 patients are considered. After the model order is determined (i.e. K and l), we examine different choices of μ, and find that $\mu = 0.001$ is the best learning rate which does not cause divergence in any of the 12 patients' respiration signals under consideration. Therefore, in our simulation, the value of μ is chosen to be 0.001.

The LMS algorithm has low computational complexity. However, its convergence rate is slow. Since, in our study, the forward prediction needs to be performed in real time, a faster convergence rate is desired. Therefore, we examine the RLS algorithm, which is a quadratic adaptive filter. Compared with LMS, the RLS algorithm has higher computational complexity, but a much faster convergence rate. The summary of the RLS algorithm is as follows.

- Initialization of the RLS algorithm is done by setting

$$\mathbf{P}(0) = \delta^{-1}\mathbf{I}$$
$$\hat{\mathbf{w}}_l(0) = 0$$

  where δ is a small positive number.
- For each time point, $i = 1, 2, \ldots$, compute

$$\mathbf{k}(i) = \frac{\lambda^{-1}\mathbf{P}(i-1)\,\mathbf{d}(i)}{1 + \lambda^{-1}\,\mathbf{d}^H(i)\mathbf{P}(i-1)\,\mathbf{d}(i)}$$
$$\xi(i) = d(i+l) - \hat{\mathbf{w}}_l^H(i-1)\,\mathbf{d}(i)$$
$$\hat{\mathbf{w}}_l(i) = \hat{\mathbf{w}}_l(i-1) + \mathbf{k}(i)\xi(i)$$
$$\mathbf{P}(i) = \lambda^{-1}\mathbf{P}(i-1) - \lambda^{-1}\mathbf{k}(i)\,\mathbf{d}^H(i)\mathbf{P}(i-1)$$

where $0 < \lambda \leqslant 1$ is the forgetting factor. With the forgetting factor, the RLS algorithm gradually forgets the history observations, and weight the recent observations more when estimating the AR coefficients. When the value of λ is close to 1, the value of λ has little effect on the prediction performance. In our study, the value of λ is chosen to be 0.99.

Although the μ and λ parameters for the LMS and RLS algorithms are predetermined, both algorithms operate in an on-line fashion. At each time point, based on the past and current observed respiration signals, both the LMS and the RLS algorithms adaptively update the estimated AR coefficients. The updated AR coefficients are then used to predict the future time points of the respiration signal. Therefore, both LMS and RLS adaptively estimate the AR coefficients and predict future time points in real time.

2.2.3. Order selection and signal autocorrelation. In an AR model, one key issue is order selection, i.e., the selection of parameters K and l in equation (2). The question becomes how many past sampled points are needed to predict an appropriate number of future points. Order selection is an important question, because low model order may result in a lack of prediction accuracy, while a high model order may result in overfitting.

Since the AR model utilizes the correlation between different time points for prediction, we first study this correlation by examining the autocorrelation. In the respiration signal, each

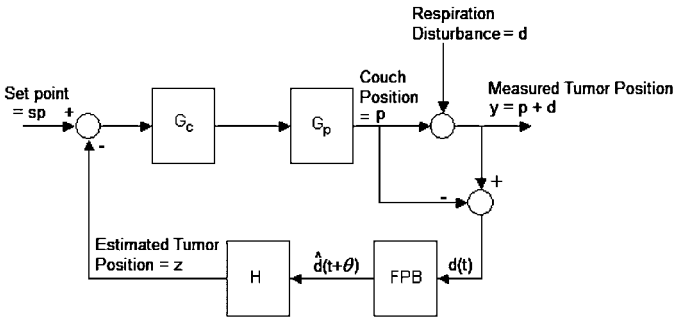

Figure 2. A block diagram incorporating forward prediction with the feedback control system. The FPB block represents the forward prediction block. It predicts the future $(t + \theta)$ disturbance based on current (t) and past observations. θ equals the dead time in the couch system.

time point can be considered as a random variable. The autocorrelation $R(k)$ (defined as the correlation between two time points with time lag k) is defined as follows:

$$R(k) = \frac{E[(d(i) - \bar{d})(d(i+k) - \bar{d})]}{\sigma^2} \tag{3}$$

where $\bar{d}$ and σ^2 are the mean and variance of the respiration signal, and E represents the expectation operation. Based on experimentally measured respiration data, the autocorrelation can be estimated:

$$R(k) = \frac{\frac{1}{N-k}\sum_{i=1}^{N-k}(d(i) - \bar{d})(d(i+k) - \bar{d})}{\frac{1}{N}\sum_{i=1}^{N}(d(i) - \bar{d})^2} \tag{4}$$

where N is the total number of time points in the respiration signal data set. From the autocorrelation, we are able to get an idea of the temporal correlation in the respiration signals and the number of consecutive time points that share enough correlation.

To determine the order of the AR model, we examine different choices of the model order and the number of future points to be predicted, using both LMS and RLS algorithms. The mean square error (MSE) was used to measure the prediction performance. Based on prediction performance, we determine the appropriate model order for predicting the respiration signal, which is how many history time points are needed to effectively predict the number of time points into the future.

2.2.4. Predictive feedback control system. The main components of a treatment couch-based feedback control system include the controller and couch. We have previously described an analysis of the controller and couch dynamics using the treatment couch to compensate for respiration-induced motion using pure feedback control (D'Souza and McAvoy 2006) and we will only briefly summarize below. Here, we propose to integrate forward prediction using LMS and RLS prediction algorithms with pure feedback control to overcome system dead time (referred to as predictive feedback control). As illustrated in figure 2, different from the previously examined feedback control system (see figure 2 in D'Souza and McAvoy (2006)), the proposed system has an additional forward prediction block (FPB). In figure 2, p represents the spatial position of the couch; y represents the spatial measurement of a skin-based sensor, which is the sum of the couch position p and the respiration-induced disturbance d; z represents the estimated tumor position with respect to the couch; sp represents the set point or desired spatial position of the tumor, which is set to be 0 relative to the desired location in the room

coordinate system; G_p is the transfer function (the transfer function is defined as the ratio between the Laplace transforms of the output and input) that represents the dynamics of the couch; G_c represents the transfer function for the feedback controller, which is designed according to the couch dynamics; H represents the conversion from the skin-based sensor displacement measurement to the tumor position. The value of the gain of H is set to 1 in this section since the skin marker was considered an exact surrogate of the tumor motion.

The transfer function for the couch, modeled as a second-order system with dead time can be written as

$$G_p = \frac{e^{-\theta s}}{(\tau_t s + 1)^2} \tag{5}$$

where θ is the dead time, and τ_t represents a time constant, which describes how fast the couch dynamics are. In equation (5), we can see that the couch system contains two parts, an invertible part $1/(\tau_t s+1)^2$ and a non-invertible part $e^{-\theta s}$. To reverse the effect of the invertible part, the control system can be designed as $G_c = (\tau_c s + 1)^2$. However, in practice, the couch is not exactly a second-order system, and there will be estimation errors in identifying the time constant, causing a model mismatch between the couch and the controller (details can be found in D'Souza and McAvoy (2006)). In our simulation, to simulate the model mismatch, the following approach is taken. Although the couch is described by second-order dynamics, the controller is designed as a first-order system, with a transfer function as follows,

$$G_c = \tau_c s + 1 \tag{6}$$

where τ_c is the controller time constant (this represents one approach for modeling a plant-model mismatch in control systems).

The non-invertible part of the transfer function describing the couch dynamics represents a dead time between the input and output of the couch system. The FPB predictor operates in real time, predicting θ seconds into the future. After we take control action to compensate this future disturbance, the control action affects the couch position after a time period θ, which is the time when the predicted disturbance occurs. The performance of the predictive feedback control system was compared with pure feedback control by evaluating motion.

2.3. Inferential predictive feedback system

In sections 2.1 and 2.2, we investigate two aspects of the real-time tumor motion compensation system (PLS and FPB) separately. In this section, we integrate the two proposed components into the feedback control system, in order to evaluate the overall performance of the motion compensation system. Multiple external skin markers are used to infer the position of the diaphragm using PLS (section 2.1) and this estimated diaphragm position serves as the input for the FPB using RLS filtering (section 2.2). The PLS inference model and the predictive feedback control method can be incorporated into one system, as illustrated in figure 3.

Since the data from section 2.1 were acquired with temporal resolution of 3.33 ms, these data were pre-processed (upsampled) by linearly interpolating the data to yield a temporal resolution of 33.37 ms (prior to any real-time inferential predictive feedback control simulations). The reason for the upsampling is that in reality one would utilize data with similar temporal resolution in the inferential model and the predictive feedback control system. Using the upsampled data, the inferential predictive feedback system was simulated as a real-time system.

The PLS inference model (in section 2.1) requires a short training period to learn the correlation between the positions of the external markers and the position of the internal anatomy. Since the correlation between external markers and internal anatomy is time varying,

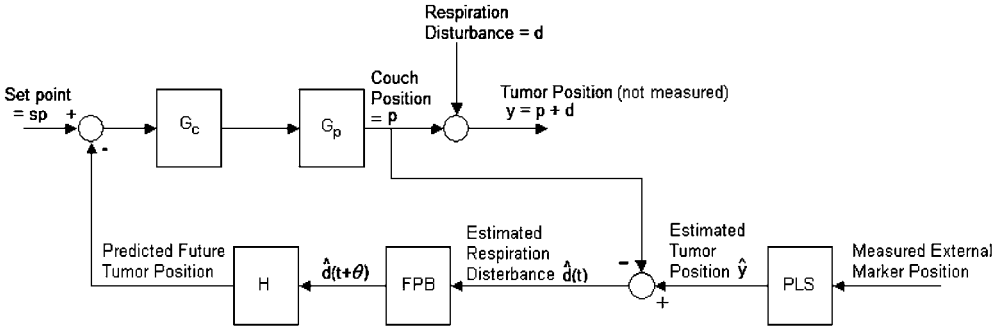

Figure 3. A block diagram of the inferential predictive feedback control system, which integrates the PLS inference model and the predictive feedback control method.

in real-time applications, the PLS model needs to be re-trained from time to time. Therefore, in the inferential predictive feedback system, the operation begins with a short training period where both the positions of the external markers and the position of the internal anatomy are measured. The measurement of the internal anatomy was the S–I position of the diaphragm position as in section 2.1. The training period is followed by a testing period. In the testing period, only the positions of the external markers are measured, and the PLS model is applied to infer the tumor position from the position of external markers. The training period and testing period alternate, so that the PLS model is re-trained periodically, to follow the time-varying correlation between the external markers and the internal anatomy.

In order to predict the future respiration disturbance, the forward prediction block relies on the respiration disturbance signal's temporal correlation, which is also time varying. However, the forward prediction component does not require periodical training, because the RLS algorithm is an adaptive scheme which can adjust itself to follow the time-varying temporal correlation of the respiration disturbance.

In summary, the PLS model predicts the position of the diaphragm in real time using the coordinates of multiple external markers and the FPB block uses RLS filtering to determine the diaphragm position in advance. The control system was simulated as described previously with a second-order with the dead time model for the couch and a first-order model for the controller. By combining the inferential modeling and the forward prediction, we evaluate the overall performance of the couch-based motion compensation system.

3. Results

We present results from (1) inferential modeling of the diaphragm position using multiple external markers, (2) predictive feedback control using LMS and RLS filters (without inferential modeling) and (3) overall performance of the feedback control system using inferential modeling and forward prediction of time-varying internal anatomical position.

3.1. Inferential modeling of the diaphragm position

Figure 4 shows one example of the time-varying displacement of the radio-opaque markers and the diaphragm. Each of the markers was displaced by different amounts but shows correlation with the diaphragm displacement. The differences in the behavior of each independent variable are expected since they correspond to markers placed at different locations on the abdomen.

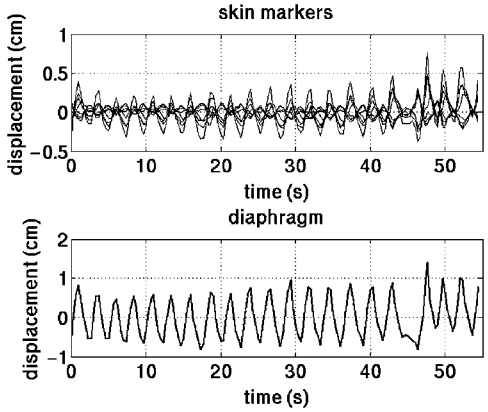

Figure 4. Overlay of the time-varying eight independent variables corresponding to the 2D coordinates of the four radio-opaque markers placed on the abdomen (top panel) and the corresponding diaphragm displacement in the S–I direction.

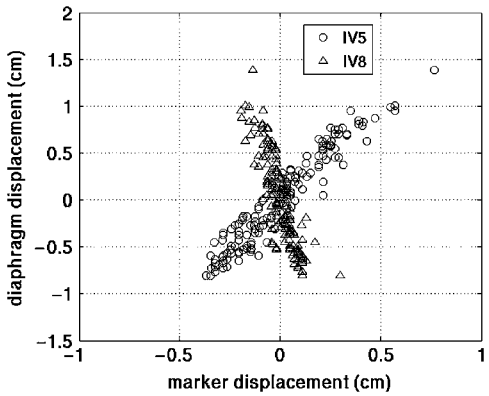

Figure 5. Relationship between the displacement of two independent variables (IV5 and IV8) and the diaphragm position. Note that the skin markers and the diaphragm are linearly related.

The skin markers were generally linearly correlated with the diaphragm position (see figure 5 for an example). The maximum peak-to-peak displacement of the diaphragm averaged over five patients was 1.7 cm with a standard deviation of 0.9 cm.

The optimal number of LVs was determined by finding the LVs resulting in the lowest cumulative PRESS in each of the sub data block into which the entire data block was split. We found that the choice of the cross-validation process (contiguous or random blocks in the training data set) did not influence the optimal number of LVs (or the cumulative PRESS error) to be used in the PLS regression model. Generally, the optimal number of LVs needed to predict the S–I diaphragm position using the anterior–posterior and lateral coordinates of the external markers was 2–3.

Once the number of LVs was determined, the key question was: how well do the skin markers predict the position of the diaphragm based on past history? Predictions of the diaphragm displacement using PLS were not influenced appreciably by the pre-processing of the data. Mean-centering the data alone generally produced prediction errors that were slightly

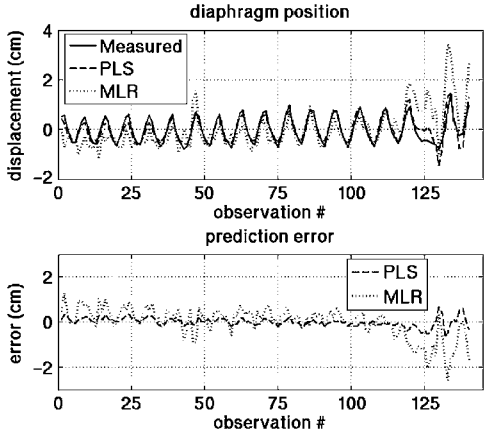

Figure 6. Comparison of the prediction of the diaphragm position using PLS and MLR with the measured diaphragm position for patient 1. While the prediction using PLS is generally good, the prediction using MLR breaks down with large errors in the range of observations 120–135.

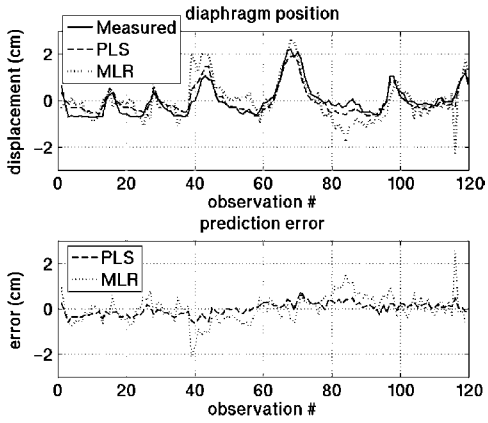

Figure 7. Comparison of the prediction of the diaphragm position using PLS and MLR with the measured diaphragm position for patient 3. The MLR prediction errors were large around observations 40, 85 and 115.

better than those produced by mean-centering and scaling to the unit variance (difference in prediction errors <0.5 mm). Figure 6 shows a comparison of the prediction of the diaphragm position using PLS and MLR with the measured diaphragm position for patient 1. The temporal resolution of each observation is 3.33 ms. Note that the PLS prediction rivals the actual measurement more closely than MLR. Figure 7 shows another example of the comparison between the PLS and MLR predictions along with the actual measured diaphragm displacement for patient 3. In both cases, the MLR breaks down particularly (in the range of observation numbers 120–135 in figure 6 and 40, 85 and 115 in figure 7) when the breathing becomes erratic while PLS was better able to predict the variations in breathing patterns.

Table 1 summarizes the mean and standard deviation of the diaphragm displacement prediction errors using LVs determined by the contiguous and random block cross-validation methods and applied to the remaining data set for each patient. Note that these values correspond to the average mean and standard deviation calculated by considering the errors

Table 1. Summary of prediction errors of the diaphragm location using PLS and MLR using LVs obtained by performing cross-validation using the *contiguous* and *random* block methods (σ is the standard deviation of the error).

	PLS (*contiguous*)		PLS (*random*)		MLR	
Patient no.	Mean (mm)	σ (mm)	Mean (mm)	σ (mm)	Mean (mm)	σ (mm)
1	1.7	2.9	1.8	2.3	3.5	3.9
2	1.5	2.1	1.6	1.8	4.2	5.0
3	2.8	3.7	3.2	3.0	10.5	11.0
4	3.3	4.9	3.9	4.7	6.4	11.1
5	0.8	1.0	1.0	1.1	1.9	2.3
Average	2.0	2.9	2.0	2.9	5.3	10.9

from using the PLS models built with each 'training' data set and applied to the remaining data set. Also shown are the corresponding mean and standard deviation of the prediction errors obtained using MLR. The mean prediction error averaged over five patients was 2.0 mm ($\sigma = 2.9$ mm) using PLS while the corresponding mean prediction error was 5.3 mm ($\sigma = 10.9$ mm) using MLR. There was no significant difference between the PLS model generated using contiguous and random data blocks in the cross-validation process.

3.2. The forward prediction block

In this section, we first examine the predictability of the respiration signal alone and then evaluate the performance of the couch-based feedback control system for motion compensation (in this section we assume that the external marker is an exact surrogate of the internal anatomy) by incorporating the FPB block into the feedback control system. The data used in this section were derived from the displacement of the RPM marker block (Varian Medical Systems, Palo Alto, CA) in 12 patients. The maximum peak-to-peak displacement of the marker block averaged over the 12 patients' data in this section was 2.1 cm with a standard deviation of 0.8 cm.

3.2.1. Forward prediction of respiration signals. The autocorrelation of $R(k)$ was estimated up to time lag of 30 points (i.e., $k = 0, 1, 2, \ldots, 30$). Autocorrelation is one measure of whether a past value can be used to predict a future value. The mean and standard deviation of $R(k)$ across the 12 data sets are shown in figure 8. It is easy to see that the autocorrelation $R(0)$, the correlation between $d(i)$ and itself, is always 1, because $d(i)$ is always perfectly correlated with itself. As k increases, the autocorrelation $R(k)$ decreases, which means nearby time points are more correlated than faraway time points. From figure 8, we can also observe that, as k increases, the standard deviation of $R(k)$ increases. This is due to the variability in breathing periods among patients. From figure 8, for time lag $k = 1, 2, \ldots, 8$, the autocorrelation was larger than 0.9 and its standard deviation was less than 0.05. Therefore, we conclude that if we want to predict $d(i)$, we can use its eight closest previous time points for the prediction.

To select the appropriate order of the AR model in equation (2), we examined the performance of both LMS and RLS algorithms with different choices of model order (K) and the number of future time points to be predicted (l). Tables 2 and 3 summarize the prediction error using the LMS and RLS algorithms, respectively. The prediction accuracy was measured by the mean square error (MSE), which was defined as $MSE = \sum_{i=1}^{N} (\hat{d}(i) - d(i))^2/N$. From these two tables, we conclude that the RLS algorithm provides a higher prediction accuracy

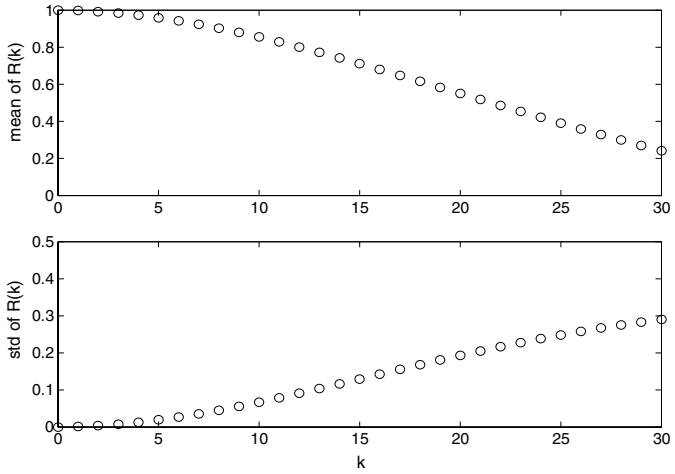

Figure 8. The mean and standard deviation of autocorrelation $R(0)$ up to $R(30)$ across marker displacements obtained from 12 patients.

Table 2. Average performance (over 12 data sets) of the LMS filter as a function of model order, (K) and the number of future points predicted (l). The prediction accuracy is measured by the mean square error (MSE). Lower MSE represents higher prediction accuracy. The unit of each entry is cm^2.

$K\backslash l$	1	2	3	4	5	6	7	8
2	0.0028	0.0050	0.0082	0.0122	0.0169	0.0223	0.0283	0.0347
3	0.0027	0.0048	0.0076	0.0111	0.0153	0.0200	0.0252	0.0309
4	0.0026	0.0044	0.0068	0.0098	0.0134	0.0174	0.0219	0.0268
5	0.0025	0.0041	0.0061	0.0087	0.0118	0.0153	0.0193	0.0236
6	0.0023	0.0038	0.0056	0.0079	0.0106	0.0138	0.0173	0.0212
7	0.0022	0.0035	0.0052	0.0073	0.0098	0.0127	0.0159	0.0196
8	0.0021	0.0033	0.0049	0.0068	0.0092	0.0119	0.0150	0.0184

Table 3. Average performance (over 12 data sets) of RLS as a function of model order (K) and the number of future points predicted (l). The prediction accuracy is measured by the mean square error (MSE). Lower MSE represents higher prediction accuracy. The unit of each entry is cm^2.

$K\backslash l$	1	2	3	4	5	6	7	8
2	0.0003	0.0010	0.0020	0.0033	0.0054	0.0079	0.0107	0.0143
3	0.0003	0.0010	0.0018	0.0031	0.0050	0.0073	0.0100	0.0135
4	0.0002	0.0008	0.0016	0.0027	0.0044	0.0066	0.0092	0.0125
5	0.0002	0.0008	0.0016	0.0027	0.0044	0.0066	0.0091	0.0124
6	0.0002	0.0008	0.0016	0.0027	0.0044	0.0065	0.0091	0.0123
7	0.0002	0.0007	0.0015	0.0026	0.0043	0.0065	0.0090	0.0122
8	0.0002	0.0007	0.0015	0.0026	0.0043	0.0064	0.0090	0.0122

than the LMS algorithm. This is because RLS has a much higher convergence rate than LMS. Therefore, RLS is able to better track the time-varying respiration signal.

If we examine table 3 column by column, we can see that for a fixed choice of l, a higher model order leads to a higher prediction accuracy. However, when the model order is too

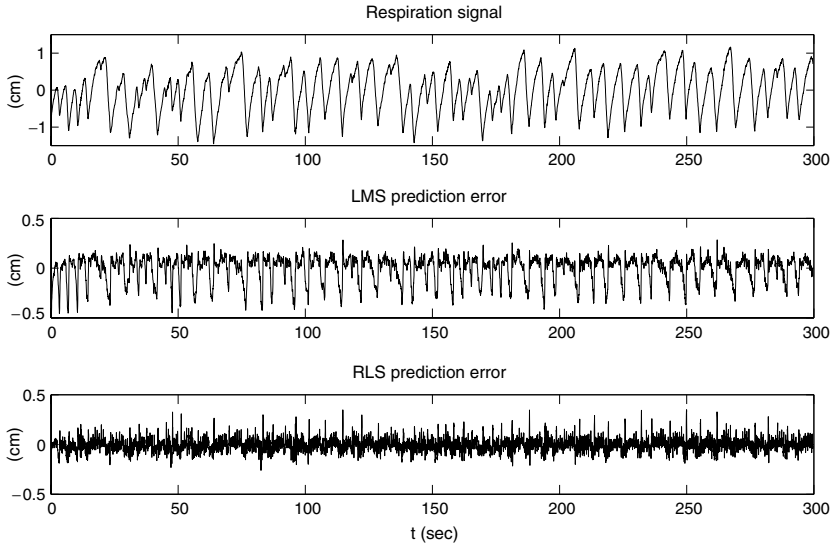

Figure 9. Prediction error for an AR model of order 4 in which six future time points are predicted. The top plot is the marker displacement signal, the middle plot is the LMS prediction error, and the bottom plot is the RLS prediction error.

high, the performance gain saturates. Therefore, a reasonable choice of model is $K = 4$. Increasing the model order from $K = 4$ does not result in a significant gain in the prediction accuracy. Another observation from table 3 is that, the prediction performance degrades if we predict far into the future. This observation is consistent with the autocorrelation presented in figure 8. The autocorrelation is small between faraway time points, which means that the current and past time points do not contain enough information about faraway future points, thus resulting in a low prediction accuracy. From table 3, it can be observed that with the model order $K = 4$, we are able to effectively predict six time points into the future. Since the respiration signal is sampled every 33.37 ms, six time points correspond to 0.2 s.

To better illustrate the comparison between LMS and RLS, an example is shown in figure 9, where we select a representative data set, choose a model order of 4 and predict 6 time points into the future. The experimentally measured respiration signal, the LMS prediction error and the RLS prediction error are shown. From this figure, we can see that with the model order being 4, RLS can predict 6 time points into the future with reasonable performance. It is also observed that the RLS algorithm outperforms LMS.

3.2.2. Predictive feedback control. While the forward prediction of the respiration signal is interesting, the key question in this work is whether forward predicting the respiration signal enhances the performance of the feedback control system. To evaluate the performance of the feedback control system with the FPB block, we compared the predictive feedback control system performance with a pure feedback control system without prediction (i.e., without the FPB block). We compared the residual motion for four cases: (1) motion without a control system, (2) motion with pure feedback control, (3) motion with LMS predictive feedback control and (4) motion with RLS predictive feedback control.

The net tumor motion after control was quantified in terms of the average displacement (AD) and the fraction (F) of time when the tumor displacement exceeds 3 mm (the approximate

standard deviation in contouring uncertainty of soft-tissue targets within planning systems). The above terms are defined as follows,

$$AD = \frac{1}{N}\sum_{i=1}^{N}|y(i)|$$

$$F = \frac{1}{N}\sum_{i=1}^{N}1(|y(i)| > 3)$$

where $y(i)$ is the tumor displacement at time point i. N is the total number of time points in the simulation. $1(|y(i)| > 3)$ is an indicator function, and it equals 1 if the condition $|y(i)| > 3$ holds; it equals 0 otherwise.

We evaluated the performance of the predictive feedback control system by systematically varying the time constants describing the couch (τ_t) and controller (τ_c). We present results for the following three sets of system parameters: (1) $\tau_t = 0.27$ s, $\tau_c = 0.56$ s, (2) $\tau_t = 0.135$ s, $\tau_c = 0.28$ s and (3) $\tau_t = 0.068$ s, $\tau_c = 0.14$ s. Since forward prediction is intended to counter dead times, for each of the above couch/controller time constant combinations, eight dead time values ranging from 1 s down to 67 ms (multiples of 33.37 ms) were examined. For each set of couch and controller time constants and system dead times, cases of (1) no control, (2) pure feedback control and (3) LMS and RLS predictive feedback control, were compared. The average of performance measures (AD and F) for data from the 12 patients considered in this section were calculated. Figures 10(a) and (b) show the performance measures (AD and F) averaged over all patients for different control schemes (with $\tau_t = 0.27$ s, $\tau_c = 0.56$ s) as a function of dead times for the couch system. Figures 10(c) and (d) show the average performance measures for different control schemes (with $\tau_t = 0.135$ s, $\tau_c = 0.28$ s) as a function of dead times for the couch system. Figures 10(e) and (f) show the average performance measures for different control schemes (with $\tau_t = 0.068$ s, $\tau_c = 0.14$ s) versus different dead times for the couch system. In each of these figures, the solid line with no marker represents the case of no control; the line with circles represents pure feedback control, the line with squares represents LMS predictive feedback control, and the line with stars represents RLS predictive control.

From figure 10, we can see that the performance with no control is constant, because it does not involve a couch system, and thus is not related to dead times. For the pure feedback control scheme, when the value of dead time is small, pure feedback control is able to compensate for the tumor motion. However, when the dead time becomes larger, pure feedback control fails because of the long delay in the couch dynamics. If the dead time is too long, pure feedback control performs even worse than the case where no control is applied. When forward prediction is incorporated into the control system, there is a significant decrease in the tumor motion, compared with the pure feedback control scheme. It is clearly observed that the RLS predictive feedback control scheme outperforms the LMS predictive feedback control scheme, because the RLS algorithm has a higher prediction accuracy than LMS. Furthermore, as the dead time increases, the performances of both LMS and RLS predictive feedback control schemes decrease. Because, when the dead time increases, the forward prediction block has to predict further into the future, which involves larger prediction errors. In summary, LMS and RLS predictive feedback control consistently outperformed a system with pure feedback control. However, LMS predictive feedback control does result in worse performance than the case of no control for dead time in the range of approximately $0.5 \sim 0.8$ s ($\tau_t = 0.27$ s, $\tau_c = 0.56$ s). Our results show that RLS predictive feedback control is therefore preferred.

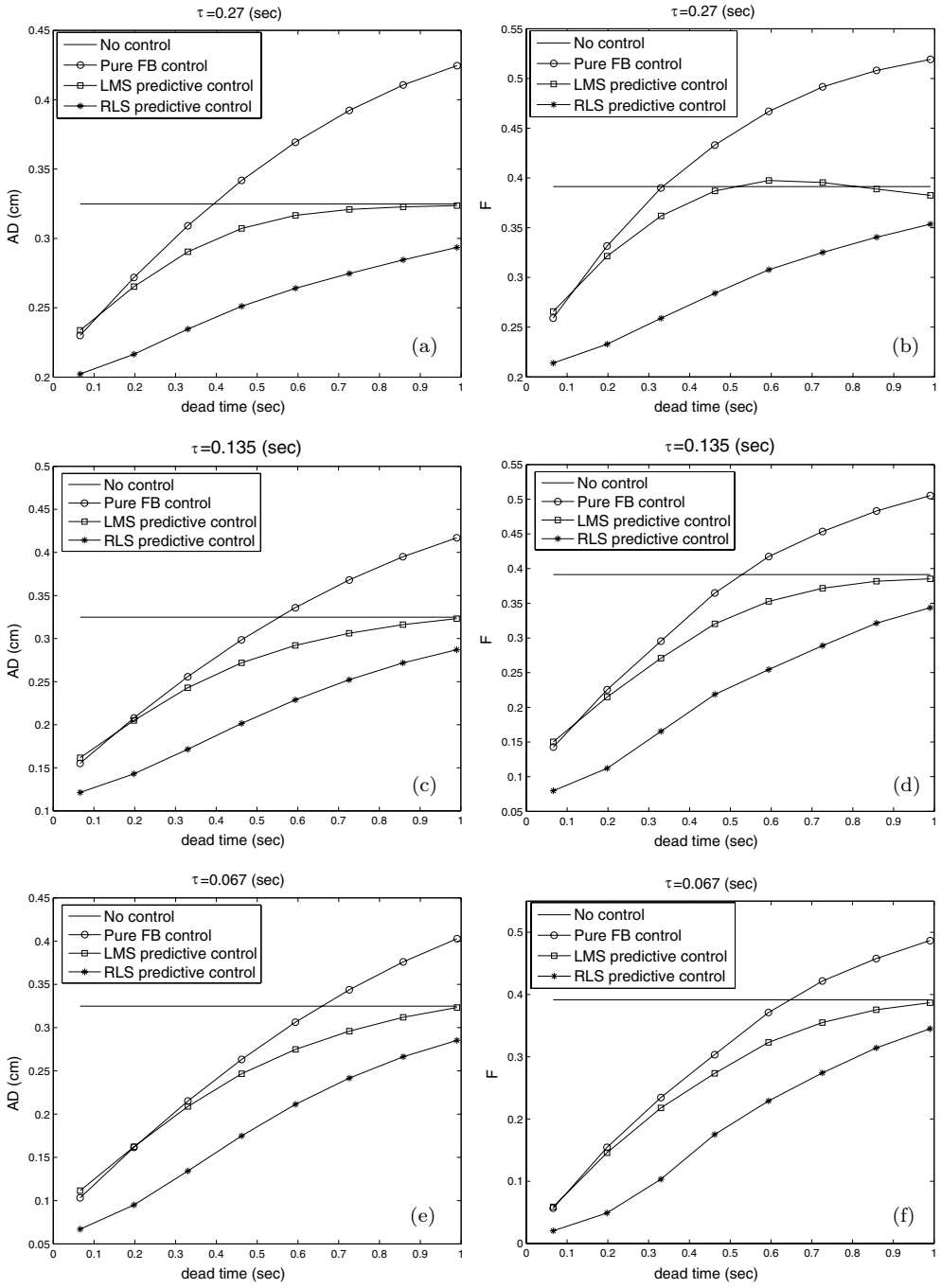

Figure 10. Average performance measures (*AD* and *F*) as a function of the couch system dead times for different control schemes with varying dynamics (i.e., τ_t and τ_c) parameters. In each of these figures, the solid line with no marker represents the case of no control; the line with circles represents pure feedback control, the line with squares represents LMS predictive feedback control, and the line with stars represents RLS predictive control.

Table 4. Performance of the control system under no control, pure FB (feedback) (with no forward prediction), LMS FB and RLS FB. Results are shown for a simulated couch system with time constant $\tau_t = 0.135$ s, $\tau_c = 0.28$ s and dead time $\theta = 0.198$ s.

$\tau = 0.135$ s $\theta = 0.198$ s	*AD* (cm)				*F*			
Patient number	No control	Pure FB	LMS FB	RLS FB	No control	Pure FB	LMS FB	RLS FB
1	0.17	0.11	0.12	0.08	0.10	0.04	0.05	0.02
2	0.35	0.21	0.21	0.14	0.52	0.27	0.26	0.09
3	0.47	0.23	0.23	0.15	0.65	0.22	0.22	0.13
4	0.40	0.26	0.27	0.17	0.62	0.40	0.36	0.17
5	0.23	0.21	0.20	0.14	0.23	0.31	0.24	0.05
6	0.13	0.11	0.11	0.07	0.06	0.01	0.02	<0.01
7	0.21	0.17	0.17	0.13	0.20	0.14	0.13	0.05
8	0.58	0.38	0.36	0.29	0.77	0.48	0.47	0.39
9	0.22	0.10	0.11	0.06	0.13	0.03	0.03	<0.01
10	0.10	0.08	0.08	0.05	0.01	<0.01	<0.01	<0.01
11	0.54	0.41	0.37	0.29	0.72	0.51	0.50	0.36
12	0.50	0.22	0.23	0.14	0.68	0.30	0.28	0.09

Table 4 summarizes *AD* and *F* for a couch system with $\tau_t = 0.135$ s, $\tau_c = 0.28$ s and $\theta = 0.198$ s. Results of four cases are shown, no control, pure feedback control, LMS predictive feedback control and RLS predictive feedback control, based on the data corresponding to the 12 patient data sets. It is observed that the RLS predictive feedback control scheme results in the lowest values for *AD* and *F*. An illustrative example is shown in figure 11, which corresponds to the fourth patient in table 4. In figure 11, the top plot shows the respiration-induced motion without any control; the second plot shows residual motion with the pure feedback control scheme; the third plot shows the residual motion with the LMS predictive feedback control scheme; and, the bottom plot shows the residual motion with the RLS predictive feedback control scheme.

3.3. Inferential predictive feedback control

We evaluated the performance of the integrated inferential predictive feedback control scheme (using RLS prediction) based on the five data sets described in section 2.1. The results for the uncontrolled diaphragm motion as well as the residual diaphragm motion using PLS inferential modeling and the predictive feedback control scheme is presented in this section.

In table 5, we show results for *AD* and *F* for inferential predictive feedback control based on the five patients' data sets. For each patient, the average error of the PLS model is presented. The average (*AD*) and the fraction (*F*) of net diaphragm displacements greater than 0.3 cm are shown in the second and third columns for the cases of no control and inferential predictive feedback control (using the RLS algorithm), respectively. The length of training and testing periods for the PLS model were fine-tuned for each data set and approximately corresponded to 1.7 s and 17 s, respectively. From this table, we can see that the PLS model and the predictive feedback control system can together reduce the respiration-induced motion. The average improvement in *AD* when inferential predictive feedback control was applied was 56% in comparison to when no control was applied. The corresponding average improvement in *F* was 16%.

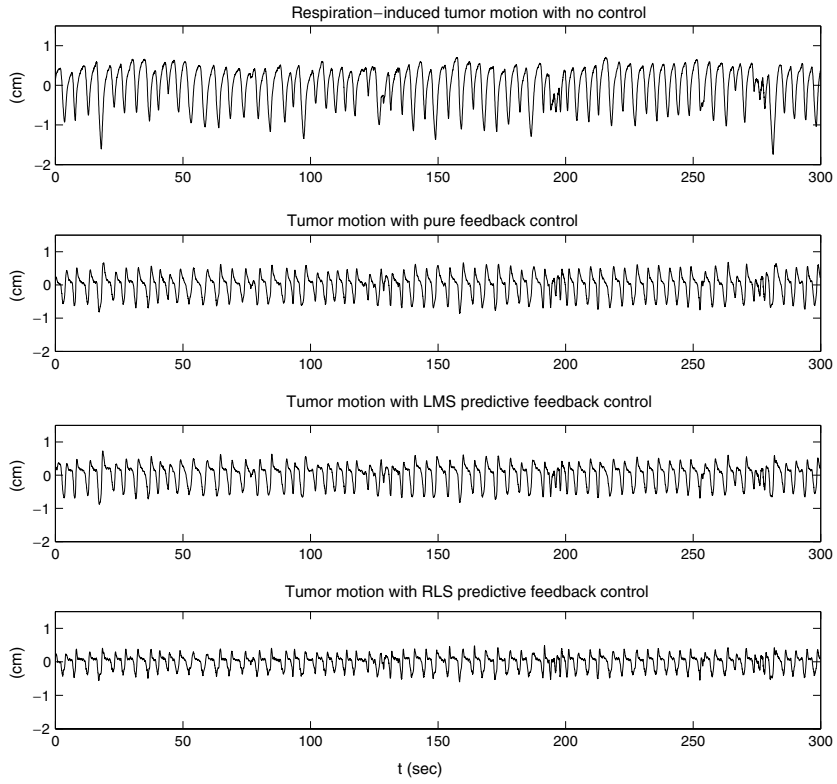

Figure 11. Illustrative example showing the prediction error (patient 4 in table 4). The top plot shows the respiration-induced tumor motion with no control; the second plot shows the tumor motion with the pure feedback control scheme; the third plot shows the tumor motion with the LMS predictive feedback control scheme; and, the bottom plot shows the tumor motion with the RLS predictive feedback control scheme.

Table 5. The uncontrolled diaphragm motion, and residual diaphragm motion with inferential predictive feedback (feedback) control schemes. Results are shown for a simulated couch system with $\tau_t = 0.135$ s, $\tau_c = 0.28$ s and $\theta = 0.198$ s.

Patient number number	PLS inference average error (cm)	Uncontrolled diaphragm motion (AD (cm))/F	PLS with RLS predictive FB (AD (cm))/F
1	0.25	0.53/0.61	0.26/0.36
2	0.14	0.39/0.64	0.30/0.52
3	0.11	0.15/0.15	0.10/0.03
4	0.08	0.15/0.04	0.10/<0.01
5	0.16	0.30/0.43	0.20/0.17

In figure 12, we show the results in the first row of table 5 in detail. For patient 1, the training and testing periods for the PLS model are chosen to be 1.7 s and 17 s, respectively. Figure 12(a) shows the measured internal diaphragm position and the PLS inferred diaphragm position. Figure 12(b) compares the measured internal diaphragm position and the residual diaphragm motion using the inferential predictive feedback control scheme. From this figure,

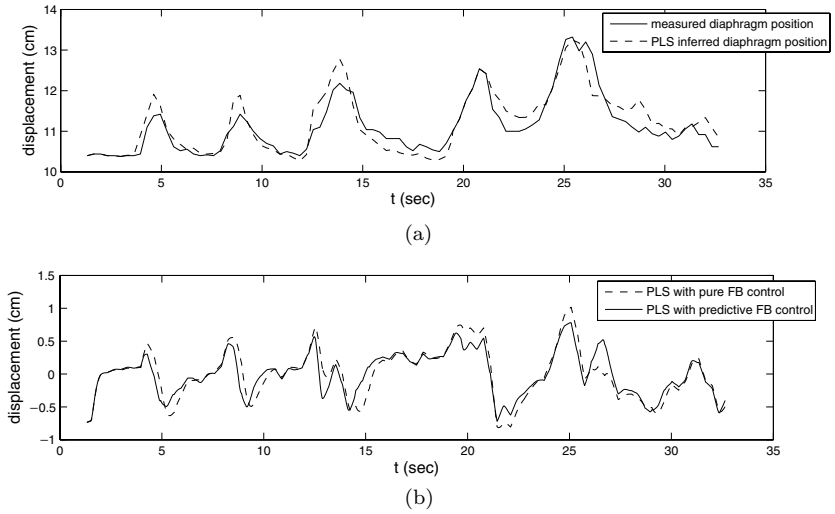

Figure 12. Figure (a) shows the measured internal diaphragm motion and the PLS inferred diaphragm motion. Figure (b) compares the measured internal diaphragm motion and the residual motion of the inferential predictive feedback control system.

we can see that, given the diaphragm position estimated by the PLS model, predictive feedback control is able to compensate the respiration-induced diaphragm motion.

4. Discussion

The goals of this paper were to (1) investigate the feasibility of using PLS to infer the time-varying diaphragm position using multiple external markers, (2) evaluate the performance of a predictive feedback control system using the LMS and RLS adaptive algorithms and (3) evaluate the performance of an integrated inferential predictive feedback control system (in which the goal was to control the respiration-induced diaphragm displacement).

Real-time tumor motion compensation using skin-based surrogates relies on a robust estimation of the tumor position by using surrogates. Furthermore, the estimation often must rely on a limited training data set consisting of a few observations and must be reliable for the course of a radiotherapy treatment fraction. Using PLS, we have shown that we can predict the diaphragm position using four radio-opaque markers placed on the abdomen with a mean error of 2.0 mm ($\sigma = 2.9$ mm) averaged over five patients. The mean prediction error using MLR was 5.3 mm ($\sigma = 10.9$ mm). We also showed that PLS outperformed MLR when predicting the diaphragm position. This outcome can be attributed to the collinearity of the input variables and the 'over-fitting' of the data in the training data set by MLR. Collinearity occurs when independent variables are so highly correlated that it becomes difficult or impossible to distinguish their individual influences on the response variable. This work has focused on predicting the diaphragm motion. These results may therefore only be extended to tumors in vicinity of the diaphragm. These tumors, interestingly, are the ones that are most susceptible to motion due to the influence of the diaphragm displacement.

If external markers are used to infer the position of the internal anatomy, we propose the following workflow. Based on our work in which a limited 'training' data set can be used to then predict the position of the diaphragm using the instantaneous positions of skin

surrogates a proposed clinical workflow could be implemented as follows. Prior to the start of each treatment fraction, a short fluroscopic movie may be acquired to delineate the internal anatomy and the external surrogates. A PLS model can then be developed which can be used to predict the real-time position of the anatomy using the instantaneous positions of the skin surrogates. While we have used radio-opaque skin surrogates, it may be more efficient to consider the use of infrared camera-based reflectors and synchronize the infrared camera acquisition with the fluoroscopic image acquisition.

As the next generation solutions (real-time motion compensation systems) for intra-fraction tumor motion are being investigated, the need for forward prediction becomes necessary in order to overcome inherent system dead times. While a few investigators have evaluated several linear filters for prediction, the limitation of previous work in this area has been a lack of evaluation of their performance in a real-time feedback control system. For example, Sharp *et al* and Vedam *et al* have shown the ability of LMS to predict the respiration signal in an open-loop setting. However, the same conclusions may not hold in a feedback system.

Two forward prediction methods were evaluated, namely the LMS and RLS filters. Our results were evaluated using the average residual displacement of the marker and the fraction of marker displacements that exceeded 0.3 cm. Irrespective of couch dynamics (described by time constants in the range of 67–270 ms), LMS and RLS filters generally improved the performance of the feedback control system in comparison with pure feedback control, and the RLS filter consistently outperformed the LMS filter. However, for some particular cases when the dead time was 0.5–0.8 s (see figure 10(b)), the LMS filter did produce inferior results when compared with the uncontrolled motion. Thus, the incorporation of the LMS algorithm into the feedback control system may degrade under certain dead time values, and produce residual tumor motion that is inferior to the uncontrolled motion. On the other hand, the RLS algorithm consistently improved the performance of the feedback control system. Therefore, the RLS algorithm is preferred. To demonstrate the proposed methods in a more practical fashion, the PLS inference model and the RLS predictive feedback control method are combined into one inferential predictive feedback control system. Based on positions of skin markers, the tumor position is estimated. We show that, based on estimated tumor motion, the predictive feedback control system outperforms a pure feedback control system without prediction.

Safety assumes an even more critical role when real-time control systems are employed for real-time motion compensation. They rely on a robust relationship between the tumor surrogate and the tumor itself. Furthermore, if a forward prediction scheme is incorporated then errors in the prediction can result in errors in motion compensation. Specifically, for the couch, certain safety critical features must be incorporated into the design. If the instantaneous required velocity exceeds the 'safe' limit such as when the patient coughs or sneezes, the system can temporarily be 'halted' and the radiation turned off through an interlock system. Motion compensation may resume once normal breathing conditions return.

5. Conclusion

In this paper, we studied two aspects of a real-time tumor motion compensation system: (1) inferential modeling of the internal anatomy using external surrogates and (2) forward prediction in the control system to overcome the system dead time. Using PLS the diaphragm position was predicted with a mean error of 2.0 mm ($\sigma = 2.9$ mm) averaged over five patients using ten samples acquired at a frequency of 3 Hz. The corresponding mean prediction error using MLR was 5.3 mm ($\sigma = 10.9$ mm). Our results indicated that the proposed RLS predictive feedback control scheme has significant performance improvement compared with a

pure feedback control system without prediction. The average uncontrolled displacement was 0.32 cm with 39% of the displacements being greater than 0.3 cm. Following predictive feedback control with $\tau_t = 0.135$ s, $\tau_c = 0.28$ s and $\theta = 0.198$ s, the average displacement was reduced to 0.14 cm, with 11% of the displacements being >0.3 cm. When PLS inferential modeling and RLS predictive feedback control were combined, the average *AD* and *F* improvements were 56% and 16%, respectively, compared with the uncontrolled diaphragm motion.

Acknowledgments

This work was supported in part by grants from the NIH/NCI, CA122403 and 3DLine Medical Systems (Milan, Italy).

References

Chang S D and Adler J R 2001 Robotics and radiosurgery—the cyberknife *Stereotact. Funct. Neurosurg.* **76** 204–8

Covey A M, Gandhi R, Brody L A, Getrajdman G, Thaler H T and Brown K T 2004 Factors associated with pneumothorax and pneumothorax requiring treatment after rercutaneous lung biopsy in 443 consecutive patients *J. Vasc. Interven. Radiol.* **15** 479–83

de Jong S 1993 SIMPLS: an alternative approach to partial least squares regression *Chemom. Intell. Lab. Syst.* **18** 251–63

Deller J R, Hanson J and Proakis J G 2000 *Discrete-Time Processing of Speech Signal* 2nd edn (Piscataway, NJ: IEEE)

D'Souza W D and McAvoy T J 2006 An analysis of treatment couch and control system dynamics for real-time compensation of motion *Med. Phys.* **33** 4701–9

D'Souza W D, Naqvi S A and Yu C X 2005 Real-time intra-fraction motion tracking using the treatment couch: a feasibility study *Phys. Med. Biol.* **50** 4021–33

Gronenschild E 1999 Correction for geometric image distortion in the x-ray imaging chain: local technique versus global technique *Med. Phys.* **26** 2602–16

Haykin S 1996 *Adaptive Filter Theory* (Englewood Cliffs, NJ: Prentice-Hall)

Imura M *et al* 2005 Insertion and fixation of fiducial markers for setup and tracking of lung tumors in radiotherapy *Int. J. Radiat. Oncol. Biol. Phys.* **63** 1442–7

Isaksson M, Jalden J and Murphy M J 2005 On using an adaptive neural network to predict lung tumor motion during respiration for radiotherapy applications *Med. Phys.* **32** 3801–9

Keall P J, Cattell H, Pokhrel D, Dieterich S, Wong K H, Murphy M J, Vedam S S, Wijesosoriya K and Mohan R 2006 Geometric accuracy of a real-time target tracking system with dynamic multileaf collimator tracking system *Int. J. Radiat. Oncol. Biol. Phys.* **65** 1579–84

Keall P J, Kini V R, Vedam S S and Mohan R 2001 Motion adaptive x-ray therapy: a feasibility study *Phys. Med. Biol.* **46** 1–10

Kinoshita F, Kato T, Sugiura K, Nishimura M, Kinoshita T, Hashimoto M, Kaminoh T and Ogawa T 2006 CT-guided transthoracic needle biopsy using a puncture site-down positioning technique *Am. J. Roent.* **187** 926–32

Lorber A, Wangen L E and Kowalsi B R 1987 A theoretical foundation for the PLS algorithm *J. Chemometr.* **1** 19–31

Murphy M J 2004 Tracking moving organs in real time *Semin. Radiat. Oncol.* **14** 91–100

Murphy M J and Dieterich S 2006 Comparative performance of linear and nonlinear neural networks to predict irregular breathing *Phys. Med. Biol.* **51** 5903–14

Naruke T and Koketsu H 1981 Transthoracic needle biopsy for lung cancer *Japan. J. Clin. Oncol.* **11** 51–60

Onimaru R, Shirato H, Fujino M, Suzuki K, Yamazaki K, Nishimura M, Dosaka-Akita H and Miyasaa K 2005 The effect of tumor location and respiratory function on tumor movement estimated by real-time tracking radiotherapy (RTRT) system *Int. J. Radiat. Oncol. Biol. Phys.* **63** 164–9

Ozhasoglu C and Murphy M J 2002 Issues in respiratory motion compensation during external-beam radiotherapy *Int. J. Radiat. Oncol. Biol. Phys.* **52** 1389–99

Papiez L 2004 DMLC leaf-pair optimal control of IMRT delivery for a moving rigid target *Med. Phys.* **31** 2742–54

Papiez L and Rangaraj D 2005 DMLC leaf-pair optimal control for mobile, deforming target *Med. Phys.* **32** 275–85

Papiez L, Rangaraj D and Keall P 2005 Real-time DMLC IMRT delivery for mobile and deforming targets *Med. Phys.* **32** 3037–48

Schweikard A, Glosser G, Boddulura M, Murphy M J and Adler J R 2000 Robotic motion compensation for respiratory movement during radiosurgery *Comput. Aided. Surg.* **5** 263–77

Schweikard A, Shiomi H and Adler J 2004 Respiration tracking in radiosurgery *Med. Phys.* **31** 2738–41

Seppenwoolde Y, Shirato H, Kitamura K, Shimizu S, van Herk M, Lebesque J V and Miyasaka K 2002 Precise and real-time measurement of 3D tumor motion in lung due to breathing and heartbeat, measured during radiotherapy *Int. J. Radiat. Oncol. Biol. Phys.* **53** 822–34

Sharp G C, Jiang S B, Shimizu S and Shirato H 2004 Tracking errors in a prototype real-time tumour tracking system *Phys. Med. Biol.* **49** 5347–56

Shimizu S, Shirato H, Ogura S, Akita-Dosaka H, Kitamura K, Nishioka T, Kagei K, Nishimura M and Miyasaka K 2002 Detection of lung tumor movement in real-time tumor-tracking radiotherapy *Int. J. Radiat. Oncol. Biol. Phys.* **51** 304–10

Shirato H *et al* 2000a Four-dimensional treatment planning and fluorosocopic real-time tumor tracking radiotherapy for moving tumor *Int. J. Radiat. Oncol. Biol. Phys.* **48** 435–42

Shirato H *et al* 2000b Physical aspects of a real-time tumor tracking system for gated radiotherapy *Int. J. Radiat. Oncol. Biol. Phys.* **48** 1187–95

Shirato H, Seppenwoolde Y, Kitamura K, Onimura R and Shimizu S 2004 Intrafractional tumor motion: lung and liver *Semin. Radiat. Oncol.* **14** 10–8

Tada T, Minakuchi K, Fujioka T, Sakurai M, Koda M, Kawase I, Nakajima T, Nishioka M, Tonai T and Kozuka T 1998 Lung cancer: intermittent irradiation synchronized with respiratory motion results of a pilot study *Radiology* **207** 779–83

Vedam S S, Keall P J, Kini V R and Mohan R 2000 Determining parameters for respiration-gated radiotherapy *Med. Phys.* **228** 2139–46

Vedam S S, Keall P J, Docef A, Todor D A, Kini V R and Mohan R 2004 Predicting respiratory motion for four-dimensional radiotherapy *Med. Phys.* **31** 2274–83

Vedam S S, Kini V R, Keall P J, Ramakrishnan V, Mostafavi H and Mohan R 2001 Quantifying the predictability of diaphragm motion during respiration with a noninvasive external marker *Med. Phys.* **30** 505–13

Webb S 2005 The effect on IMRT conformality of elastic tissue movement and a practical suggestion for movement compensation via the modified dynamic multileaf collimator (dMLC) technique *Phys. Med. Biol.* **50** 1163–90

Wijesooriya K, Bartee C, Siebers J V, Vedam S S and Keall P J 2005 Determination of maximum leaf velocity and acceleration of a dynamic multileaf collimator: implications for 4D radiotherapy *Med. Phys.* **32** 932–41

Wold S, Ruhe A, Wold H and Dunn W J III 1994 The collinearity problem in linear regression: the partial least square approach to generalized inverses. *SIAM J. Sci. Stat. Comput.* **5** 735–43

Yan H, Yin F F, Zhu G P, Ajlouni M and Kim J H 2006 The correlation evaluation of a tumor tracking system using multiple external markers *Med. Phys.* **33** 4073–84